



HAL
open science

Monitoring and Assessing Iridium-Promoted Photoredox Catalysis by Electrochemistry

Julie Quintaine, Lionel Saudan, Francesco Santoro, Gilles Oddon, Eric Labbé,
Olivier Buriez

► **To cite this version:**

Julie Quintaine, Lionel Saudan, Francesco Santoro, Gilles Oddon, Eric Labbé, et al.. Monitoring and Assessing Iridium-Promoted Photoredox Catalysis by Electrochemistry. *ACS Catalysis*, 2023, 13 (22), pp.14894-14906. 10.1021/acscatal.3c04058 . hal-04350766

HAL Id: hal-04350766

<https://hal.science/hal-04350766v1>

Submitted on 18 Dec 2023

HAL is a multi-disciplinary open access archive for the deposit and dissemination of scientific research documents, whether they are published or not. The documents may come from teaching and research institutions in France or abroad, or from public or private research centers.

L'archive ouverte pluridisciplinaire **HAL**, est destinée au dépôt et à la diffusion de documents scientifiques de niveau recherche, publiés ou non, émanant des établissements d'enseignement et de recherche français ou étrangers, des laboratoires publics ou privés.

Monitoring and Assessing Iridium-promoted Photoredox Catalysis by Electrochemistry

Julie Quintaine,^{b,‡,} Lionel Saudan,^{b, ‡} Francesco Santoro,^{b, ‡} Gilles Oddon ^{c, ‡} Eric Labbé,^{a, ‡}
Olivier Buriez,^{a, ‡, *}*

^a PASTEUR, Département de Chimie, Ecole Normale Supérieure, PSL University, Sorbonne Université, CNRS, 75005 Paris, France.

^b Discovery chemistry & Development, Research & Development, dsm-firmenich, 7 rue de la Bergère, CH-1242 Satigny, Geneva, Switzerland.

^c Ingredients, Perfumery & Beauty, dsm-firmenich, 7 rue de la Bergère, CH-1242 Satigny, Geneva, Switzerland.

KEYWORDS. Photoredox Catalysis; Iridium; Electrochemistry; Mechanistic investigations; Photochemistry; Organocatalysis; Hydrogen-atom transfer.

ABSTRACT.

Recently, Professor David MacMillan introduced an original light-mediated catalytic process where simple aldehyde substrates undergo coupling with a variety of olefin partners to enantioselectively afford α -alkyl carbonyl adducts. Based on the redox potential values reported for some transient intermediates and on the knowledge-based reactivity of organic radicals, it was suggested that the alkylation of aldehydes proceeds along merged photoredox, organic, and hydrogen-atom transfer (HAT) catalytic sub-cycles. Inspired by this seminal work, we undertook an electrochemical investigation of the mechanism of the blue light-mediated coupling of propanal with β -pinene. The coupling reaction was performed in dimethoxyethane, using $\text{Ir}(\text{dF}(\text{CF}_3)\text{ppy})_2(\text{dtbbpy})](\text{PF}_6)$ as the photoredox catalyst, *N*-methyl-trifluoroethanamine as the enamine catalyst precursor, and 2,4,6-triisopropylbenzenethiol (ArSH) as the hydrogen atom transfer agent. Under these conditions, cyclic voltammetry and chronoamperometry allowed: (a) the determination of the redox potential values of most intermediates involved in the three catalytic cycles, including the iridium complex under its ground and excited states, (b) to evidence the *in-situ* formation of the enamine catalyst obtained by reaction between propanal and *N*-methyl-trifluoroethanamine, (c) to estimate the equilibrium condensation constant between the aldehyde and the amine, (d) to follow the enamine oxidation by the excited iridium complex, and (e) to reveal the inter-dependence between the photoredox and the HAT catalytic cycles. Thus, the enamine concentration, monitored by chronoamperometry, accounted for every change on the three catalytic sub-cycles and allowed us to assess and strengthen the occurrence of key-steps involved in the overall process. This experimental mechanistic investigation, reinforced by gas chromatography analysis of solutions obtained under synthetic conditions, fully supported

MacMillan's mechanistic framework. Electrochemical methods appear to be powerful to establish the sequence of reactions triggered by photochemical activation of iridium precursors.

INTRODUCTION.

During the last decade, visible-light initiated organic transformations have attracted increasing attention. Indeed, the development of photocatalytic reactions, which enable rapid and efficient synthesis of fine chemicals, is highly desirable from the viewpoint of cost, safety, availability, and environmental purposes. Within this context, not only transition metal chromophore such as ruthenium and iridium polypyridyl complexes clearly demonstrated their great versatility in organic synthesis,¹⁻⁷ but also organic photoredox catalysts can be useful in many synthetic transformations with a wide range of applications.⁸

Considering the rapid development of photoredox synthetic strategies and their apparent reaction complexity, robust mechanistic investigations are required to assess the catalytic sequences. So far, most reported information essentially relies on redox potential calculations, Stern-Volmer measurements, computational approaches, bond dissociation energies, and variation in reagent concentration.⁹⁻¹² Obviously, these parameters are crucial to characterize the initial steps. Nevertheless, they fail to provide a full description of the catalytic system, limiting thus possible processes improvements in terms of yields and/or reaction completion times.

Photochemical approaches are reliable to identify transient species and determine the rate constants involving the photoredox catalyst activation/quenching steps, which take place within very short time-scales.¹³⁻²⁶ For instance, the use of transient vibrational and electronic absorption spectroscopy with sub-picosecond time resolution allowed for determination of rate constants for electron transfer radical polymerization.^{13, 14} Similarly, the use of transient and steady state spectroscopic techniques allowed for characterization of transient radical intermediates and

determination of the kinetic constants related to a hydrogen atom transfer cycle involved in an alkene hydrofunctionalization reaction.¹⁵

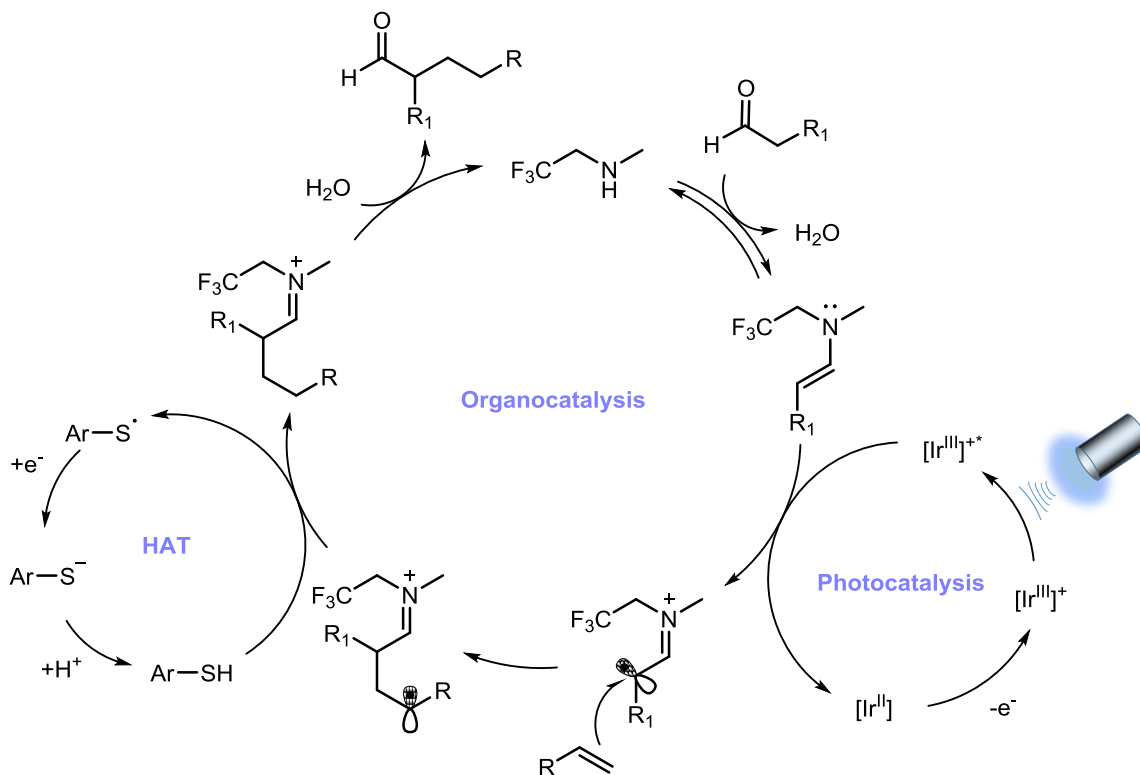
The numerous photocatalytic reactions developed by MacMillan and co-workers are interesting models of light-induced organocatalytic reactions, as shown by Swierk and co-workers²⁷ who recently investigated an α -aminoarylation photoredox reaction.²⁸ Based on a combination of steady state photochemical measurements, transient laser spectroscopy, and spectroelectrochemical methods, a comprehensive mechanistic scheme was proposed featuring productive and unproductive reaction pathways, supported by the determination of rate constants. Similarly, the same group²⁹ investigated the mechanism involved in the direct arylation of allylic sp^3 C–H bonds via organic and photoredox catalysis.³⁰

In the context of mechanistic investigations, electrochemistry should emerge as a one of the most versatile method to explore photoredox catalysis processes especially when redox species without photoluminescent properties are involved. Indeed, compared to photochemistry, electrochemical techniques allow an increase in the time-scale that can be accessed, making both approaches complementary.

Although electrochemistry has long been used to study the mechanisms of organic and organometallic reactions,³¹⁻³⁶ almost no electrochemical exploration of photoredox processes has been reported.³⁷

Among the multiple photoredox catalytic reactions developed so far, those involving merged cyclic processes are particularly interesting for the versatility of synthetic solutions they provide.^{38 - 46} The alkylation of aldehydes in the presence of olefins⁴⁶ is a typical example in which a synergistic merging of three catalytic cycles namely, photoredox, organic and hydrogen-atom transfer (HAT) cycles, respectively, as depicted in Scheme 1. This mechanistic framework

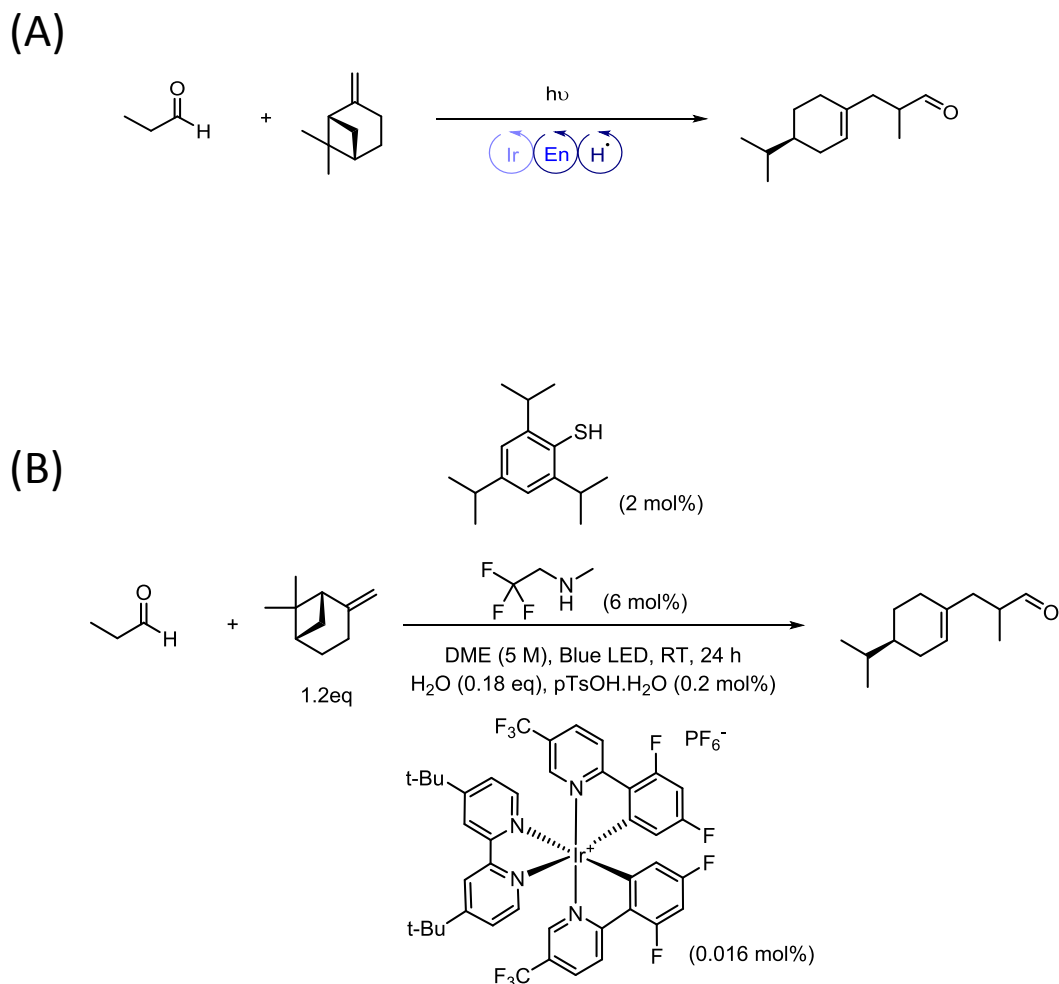
relies on the knowledge of both the redox potential values of some key species (e.g. $E_{1/2}[*\text{Ir(III)}/\text{Ir(II)}]$; $E_{1/2}[\text{PhS}^{\bullet}/\text{PhS}^-]$; $E_{1/2}[\text{Ir(III)}/\text{Ir(II)}]$) and the reactivity of organic radicals.



Scheme 1. General mechanism proposed for the blue light-mediated coupling of aldehydes with olefins.

In this work, we intended to investigate the mechanism of the visible light-mediated coupling of propanal with β -pinene from the electrochemist viewpoint, i.e. focusing on the fate of electroactive species under illumination. This transformation was of particular interest for DSM-Firmenich chemists who developed and optimized its conditions.⁴⁷ It was performed under blue-light illumination, in dimethoxyethane (DME) in the presence of acid and water, using $\text{Ir}(\text{dF}(\text{CF}_3)\text{ppy})_2(\text{dtbbpy})(\text{PF}_6)$ as the photoredox catalyst, *N*-methyl-trifluoroethanamine as the

enamine catalyst precursor, and 2,4,6-triisopropylbenzenethiol (ArSH) as the hydrogen atom transfer catalyst as displayed in Scheme 2.



Scheme 2. (A) Specific coupling reaction investigated in this work. (B) Experimental conditions of the investigated reaction.

Cyclic voltammetry brought crucial information on (a) the redox potential values of most of species involved in the three catalytic cycles including the iridium complex under its ground and excited states, (b) the *in-situ* formation of the enamine obtained by condensation of propanal and

N-methyl-trifluoroethanamine, (c) the determination of the thermodynamic constant of the condensation equilibrium between the aldehyde and the amine compounds, (d) the enamine oxidation and (e) the inter-dependence between the photoredox and the HAT catalytic cycles. Chronoamperometry allowed the monitoring of the enamine intermediate as a function of experimental conditions (presence or absence of ArSH and/or β -pinene and/or water). The electrochemical investigation was also supported by gas chromatography analysis of solutions obtained under preparative conditions. Finally, we propose a mechanistic scheme for the blue light-mediated coupling of propanal with β -pinene (See the Conclusion section), which strengthens the occurrence of a triple photochemical / organocatalytic / HAT process.

EXPERIMENTAL SECTION.

Chemicals

Tetrabutylammonium tetrafluoroborate (TBABF₄) used as the supporting electrolyte in dimethoxyethane (DME, Sigma-Aldrich) was prepared from NaBF₄ (Merck), and n-Bu₄NHSO₄ (Alfa Aesar), recrystallized from ethyl acetate-hexane (both from Sigma-Aldrich), and dried at 60 °C. Commercially available reagents were used directly without purification: propanal (Sigma-Aldrich), β -pinene (Alfa-Aesar), *para*-toluenesulfonic acid monohydrate (Sigma-Aldrich), 1-pyrrolidino-1-cyclohexene (Sigma-Aldrich), Ir(dF(CF₃)ppy)₂(dtbbpy)](PF₆),⁴⁸ 2,4,6-Triisopropylbenzenethiol,⁴⁹ bis-(2,4,6-triisopropylphenyl) disulfide,⁵⁰ *N*-methyl-trifluoroethanamine⁵¹ and *N*-isobutyl-trifluoroethanamine⁵² were prepared according to published procedures.

Instrumentation

Cyclic voltammetry and chronoamperometry experiments were performed by using an Autolab potentiostat (PGSTAT 20). A Perkin Elmer Lambda 45 spectrometer and a JASCO FP-8300 spectrofluorometer were used in absorption and fluorescence experiments, respectively. A blue led (Kessil H150 Blue) was used to trigger the photoredox reaction.

Gas chromatography (GC) was carried out on an *Agilent* 6850 instrument, using fused silica capillary columns (DB Wax, 10 m x 0.1 mm x 0.1 μm ; HP-1 30 m x 0.32 mm x 0.25 μm) and using hydrogen as carrier gas.

Cyclic voltammetry

Cyclic voltammetry experiments were performed at room temperature under argon atmosphere in a three-electrode cell using an Autolab potentiostat (PGSTAT 20). The reference electrode was a saturated calomel electrode (SCE, Radiometer), separated from the solution by a bridge compartment filled with the same solvent / supporting electrolyte solution as used in the cell. The counter electrode was a platinum wire (1 cm length, Goodfellow). The glass-sealed platinum (0.5 mm diameter, Goodfellow) or glassy carbon (1 mm diameter, Goodfellow) working electrode disks were homemade.

Steady-state chronoamperometry

Chronoamperometry experiments were performed at a platinum rotating disk electrode (RDE – Radiometer) to ensure a stationary transport regime at the electrode surface, with a potential value set at a constant value of + 1 V / SCE.

RESULTS and DISCUSSION.

1) Redox properties of the iridium complex in DME

The redox properties of the iridium complex catalyst were first investigated in dimethoxyethane (DME), used as solvent in the original synthetic developments. In this medium, the electrochemical behavior of the iridium complex, $\text{Ir}(\text{dF}(\text{CF}_3)\text{ppy})_2(\text{dtbbpy})](\text{PF}_6)$ (see structure in Scheme 2(B)), was similar to that described in acetonitrile⁴⁸ though some differences were observed in terms of potential values depending on the working electrode material (Table 1).

Table 1. Redox properties of $\text{Ir}(\text{dF}(\text{CF}_3)\text{ppy})_2(\text{dtbbpy})](\text{PF}_6)$ as a function of the nature of both the solvent (acetonitrile (MeCN) or dimethoxyethane (DME)) and the electrode material (platinum (Pt) or glassy carbon electrode (GCE)).

	$E^\circ (\text{Ir}^{\text{IV}}/\text{Ir}^{\text{III}})^a$	$E^\circ ([\text{IrL}_1\text{L}_2]^+ / [\text{IrL}_1\text{L}_2]^0)^b$	$E^\circ ([\text{IrL}_1\text{L}_2]^0 / [\text{IrL}_1\text{L}_2]^-)$
MeCN / Pt electrode ^c	+ 1.69	-1.37	-1.68
MeCN / GCE	+ 1.83	-1.36	-1.70
DME / GCE	+ 2.00	-1.12	-1.71

^aPotential values are given in volts versus SCE. ^b $L_1 = \text{dtbbpy}$; $L_2 = \text{dF}(\text{CF}_3)\text{ppy}$. ^cValues obtained from reference (48).

In acetonitrile (MeCN), similar potential values were obtained at platinum (Pt) or glassy carbon electrode (GCE) except for the oxidation of the Ir(III) metal center to Ir(IV) that was slightly more positive at GCE (+1.83 instead of +1.69 on Pt). In DME, the latter oxidation was observed at +2.00 V on GCE (i.e. a potential value overlapping the solvent oxidation) in agreement with a stronger electron-donating effect of MeCN compared to DME (Figure 1(A)). Accordingly, under the same conditions (DME / GCE), the first reduction of the iridium complex (ascribed to the

reduction of the dtbbpy ligand) was observed at a less negative potential value than in MeCN (-1.12 V vs. -1.36 V) (compare wave R₁ potential values in Figures 1(B) and 1(C)). Nevertheless, the second ligand-centered redox wave corresponding to the reduction of dF(CF₃)ppy was located at a similar potential values in both solvents (around -1.70 V) independent of the electrode material, showing the absence of solvent effect in this case.

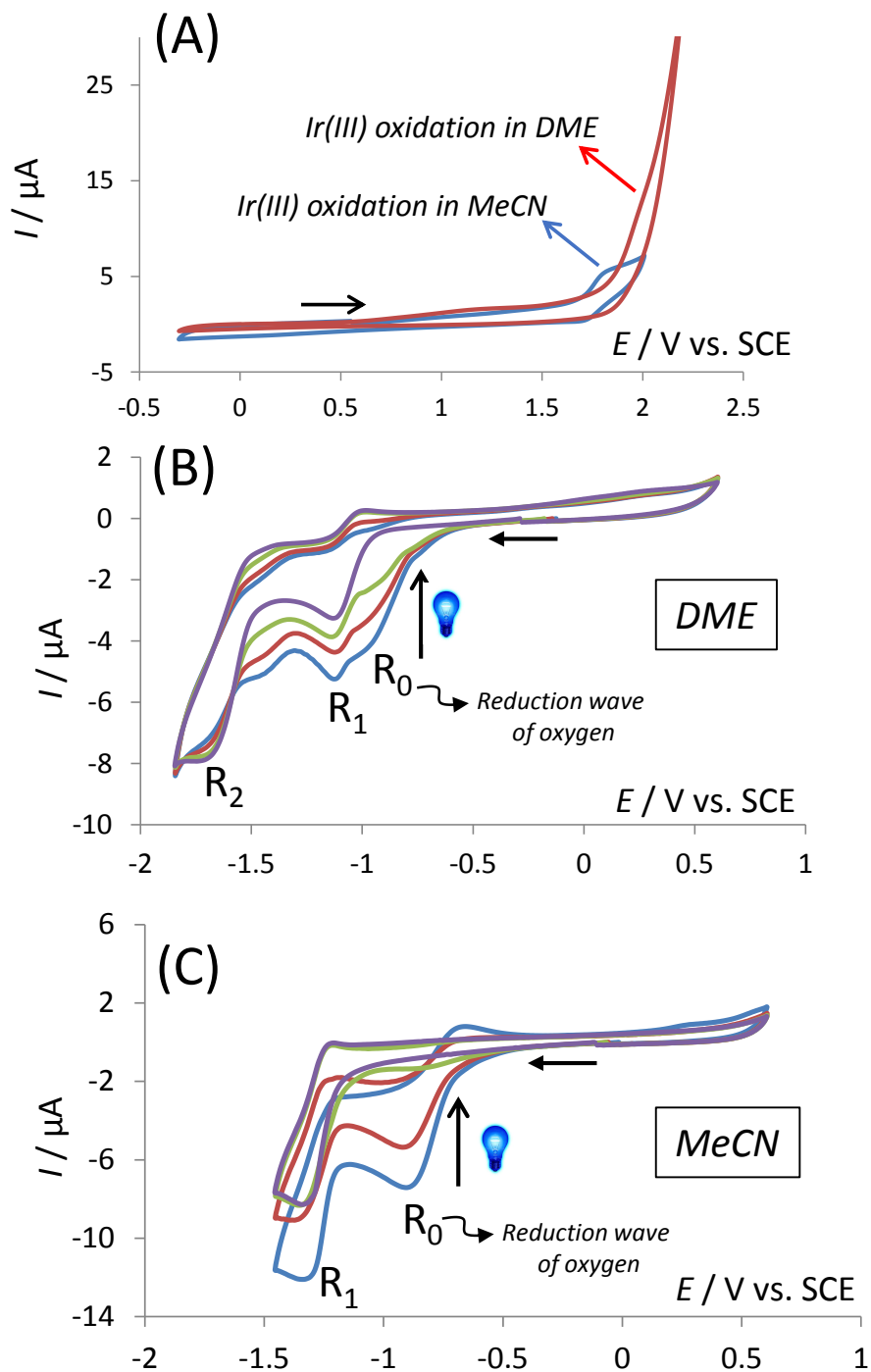
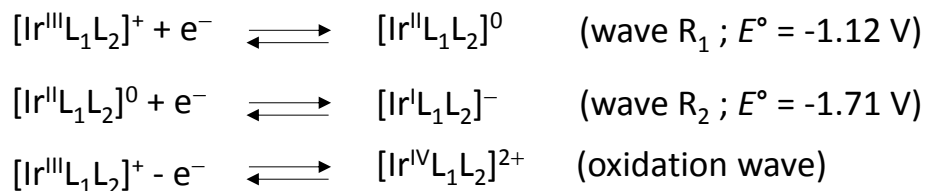


Figure 1. Cyclic voltammograms of $\text{Ir}(\text{dF}(\text{CF}_3)\text{ppy})_2(\text{dtbbpy})](\text{PF}_6)$ performed in DME/ or MeCN/[TBA][BF₄] (0.3 M) at a glassy carbon electrode (1 mm in diameter) and at a scan rate of 100 mV/s. (A) Comparison of anodic scans obtained in DME or MeCN (Iridium complex concentration: 1.18 mM in DME and 1 mM in MeCN); (B) Cathodic scan of the iridium complex (1.18 mM) in DME, without and under blue light illumination; (C) Cathodic scan of the iridium complex (1.21 mM) in MeCN – effect of the blue light illumination when *N*-methyl-trifluoroethanamine (12.10 mM) was present in solution.

In Scheme 3 are shown the two main reduction processes of the iridium complex in DME.



Scheme 3. Reduction processes of the complex $\text{Ir}(\text{dF}(\text{CF}_3)\text{ppy})_2(\text{dtbbpy})](\text{PF}_6)$ in DME.

In addition to electro-analyses carried out on the iridium complex in its ground state, it was also of interest to evaluate the redox properties of its excited state in the same solvent. A good estimation of these values can be derived from the Rehm–Weller theory.⁵³ To a first approximation, the redox potentials for the excited state couples may be calculated from the potential values of the ground state couples and the zero-zero excitation energy E^{0-0} (in the Rehm-Weller equation the Coulomb term is negligible in comparison to the other terms, especially in polar solvents). E^{0-0} represents the electronic transitions between the lowest vibrational levels of the electronic states (the 0-0 transition) that have the same energy in both absorption and fluorescence. Accordingly, the E^{0-0} value (2.82 eV) was determined from the intersection point between the absorbance and fluorescence spectra whereas the excited state redox potential values were obtained from equations (1) and (2) (see S.I.).^{54,55} Note that in MeCN similar absorption and fluorescence spectra were obtained leading to a E^{0-0} value equal to 2.79 eV.

$$E^\circ (\text{Ir}^{\text{IV}} / * \text{Ir}^{\text{III}}) = E^\circ (\text{Ir}^{\text{IV}} / \text{Ir}^{\text{III}}) - E^{0-0} \quad (1)$$

$$E^\circ (* \text{Ir}^{\text{III}} / \text{Ir}^{\text{II}}) = E^\circ ([\text{IrL}_1\text{L}_2]^+ / [\text{IrL}_1\text{L}_2]^0) + E^{0-0} \quad (2)$$

In Table 2 are reported the redox values estimated for the complex $\text{Ir}(\text{dF}(\text{CF}_3)\text{ppy})_2(\text{dtbbpy})](\text{PF}_6)$ in its excited state. Obviously, these values may depend slightly upon the nature of the working electrode material (see Table 1). Interestingly, and as shown in Table 2, the reductive power of $^*\text{Ir}(\text{III})$ is similar in MeCN and DME whereas its oxidative power is stronger in the latter solvent (the more positive the potential value, the stronger the oxidant).

Table 2. Estimation of the redox values of $\text{Ir}(\text{dF}(\text{CF}_3)\text{ppy})_2(\text{dtbbpy})](\text{PF}_6)$ in its excited state

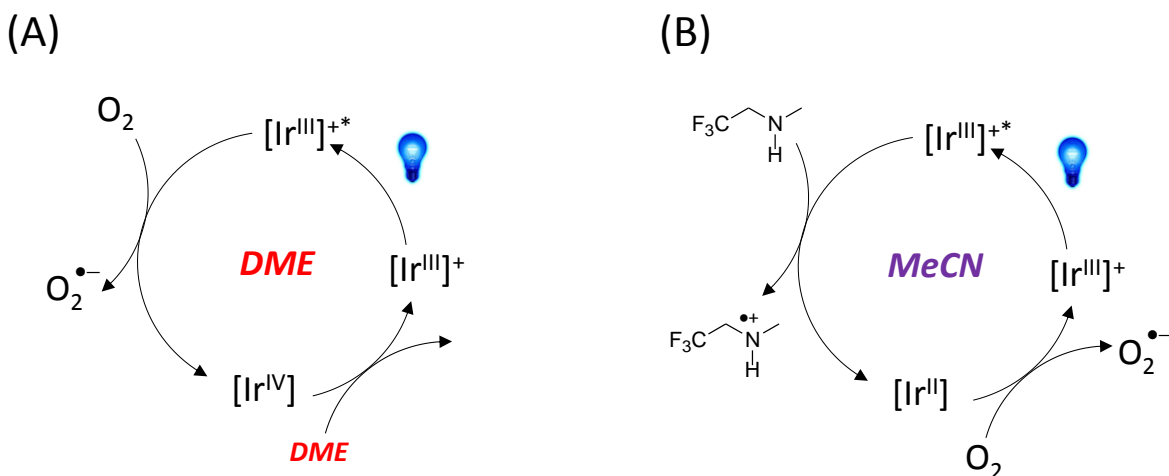
	$E^\circ (*\text{Ir}^{\text{III}}/\text{Ir}^{\text{II}})^{\text{a}}$	$E^\circ (\text{Ir}^{\text{IV}}/*\text{Ir}^{\text{III}})^{\text{a}}$
MeCN	+ 1.21 ^b / +1.46 ^c	-0.89 ^b / -0.99 ^c
DME	+ 1.70 ^c	-0.82 ^c

^aPotential values are given in volts versus SCE. ^bValues given in reference (1). ^cDetermined from the potential values obtained on a glassy carbon electrode (GCE).

2) Blue light effect on oxygen present in solution

In DME, an additional reduction process corresponding to the reduction of residual oxygen in solution was often observed (see wave R_0 at around -0.9 V in Figure 1(B)). Interestingly, we observed that illumination of the solution with a blue LED allowed elimination of oxygen more easily than bubbling argon for several minutes. As shown in Figure 1(B), the oxygen reduction wave totally disappeared after illumination of the solution. Moreover, the peak current intensities of reduction waves R_1 and R_2 (corresponding to the successive ligand-centered reduction processes of the iridium complex) remained similar after illumination indicating a regeneration of the starting $\text{Ir}(\text{III})$ ground state. From the mechanistic viewpoint, the $^*\text{Ir}(\text{III})$ excited state very likely undergoes an oxidative quenching in the presence of molecular oxygen leading to $\text{O}_2^{\bullet-}$ and $\text{Ir}(\text{IV})$. Considering the oxidation potential value of DME ($\sim +2$ V) and the E° value of the

Ir(IV)/Ir(III) couple (+ 2 V – see Figure 1(A)), the solvent may therefore be oxidized by Ir(IV) to regenerate the starting Ir(III) complex as depicted in Scheme 4(A).



Scheme 4. Possible iridium-promoted mechanisms of molecular oxygen elimination in (A) DME or (B) MeCN.

Surprisingly, this original behavior was not observed in MeCN despite similar redox properties of the Ir^{IV}/*Ir^{III} couple. This could be due to a weaker oxidation power of the Ir(IV) complex towards acetonitrile. Besides, and compared to DME, the oxidation potential of MeCN occurred at a more positive value ($E > +2$ V) than that of Ir(IV) (Figure 1(A)).

This result prompted us to investigate the reductive power of Ir(II) generated after reductive quenching of *Ir(III) in the presence of an amine such as *N*-methyl-trifluoroethanamine. Accordingly, and as shown in Figure 1(C), the reduction wave of oxygen disappeared under blue illumination only when the amine was present. Under these conditions, the *Ir(III) excited state would undergo a reductive quenching leading to the oxidation of the amine and producing an Ir(II) complex. Moreover, based on the redox potential values of both Ir(III) and oxygen in

MeCN (around -1.36 and -0.80 V, respectively), the reduction of O₂ by Ir(II) would therefore be thermodynamically favorable to regenerate the starting Ir(III) complex along with the oxygen anion radical (Scheme 4(B)).

3) Observation of the iridium reductive quenching in the presence of an in-situ prepared enamine

The α -alkylation of aldehydes is assumed to begin with the condensation between an amine and an aldehyde providing an enamine substrate. Then, irradiation of the iridium photocatalyst with blue light would produce the iridium excited state $^*[\text{Ir(III)}^+]$ that undergoes single-electron transfer from the electron-rich enamine to generate the reduced Ir(II) complex along with the enaminy radical species (Scheme 1). Although coherent, this mechanistic description lacks experimental milestones notably to address essential questions such as: (a) What is the thermodynamic equilibrium constant of the formation of the enamine? (b) What is the oxidation potential value of the enamine species? (c) Among the possible reducers/quenchers present in the reaction medium, which one (between amine, aldehyde, and enamine) will be preferentially oxidized by the iridium excited state $^*[\text{Ir(III)}^+]$? (d) what is the actual rate determining step in the iridium catalyst regeneration? Electrochemical techniques have long been established as particularly adapted to catch the faradaic signature of stable or transient redox intermediates over large timescales,⁵⁶ a property that may provide at least partial answers to these questions.

a) Assessing the enamine formation (Reaction noted as 1 in Scheme 7)

First, it was important to assess the *in-situ* formation of enamine by mixing the amine (2,2,2-trifluoro-N-methylethanamine) and the aldehyde (propanal).

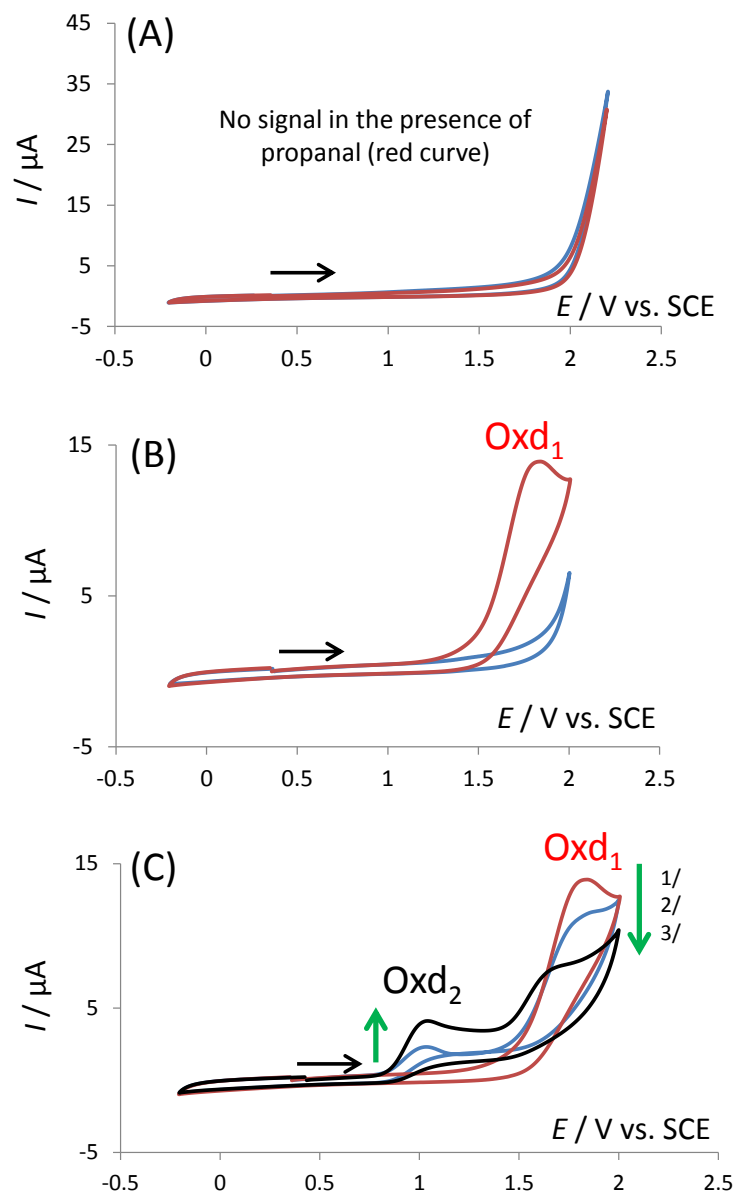


Figure 2. (A) Cyclic voltammograms of DME/[TBA][BF₄] (0.3 M) in the absence (blue) and the presence (red) of propanal (0.3 M). (B) Cyclic voltammograms of DME/[TBA][BF₄] (0.3 M) in the absence (blue) and the presence (red) of *N*-methyl-trifluoroethanamine (8.9 mM). (C) Cyclic voltammogram of *N*-methyl-trifluoroethanamine (8.9 mM) in DME/[TBA][BF₄] (0.3 M) in the absence (1/), in the presence (2/) of propanal (0.3 M), and (3/) in the presence of both propanal (0.3 M) and para-toluenesulfonic acid (1.75 mM). Conditions: studies performed at a GCE (1 mm in diameter) and at a scan rate of 100 mV/s.

As shown in Figure 2, propionaldehyde is not electroactive between 0 and + 2 V (Figure 2(A)) whereas the amine is oxidized at ca. + 1.75 V (wave Oxd₁ in Figure 2(B)). Interestingly, when the aldehyde and the amine were added to the electrochemical cell, a new oxidation wave (noted Oxd₂ in Figure 2(C)) appeared at around + 1 V. Importantly, the peak current increase of Oxd₂ was accompanied by a peak current decrease of Oxd₁, in the same scan, indicating that Oxd₂ appears and increases to the detriment of Oxd₁. Furthermore, the peak current increase and decrease of Oxd₂ and Oxd₁, respectively, became more intense in the presence of *para*-toluenesulfonic acid known to catalyze the aldehyde-amine condensation (see (C) in Figure 2). All these results indicate that propanal and 2,2,2-trifluoro-N-methylethanamine reacted to provide the corresponding enamine whose oxidation potential (~ +1 V) matches the expected value for this family of molecules.⁵⁷ From the peak current intensities at waves Oxd₁ and Oxd₂, directly representing the concentration of respectively the enamine and the amine in solution, one could roughly estimate the thermodynamic constant of the condensation $K = 1.4 \times 10^{-2}$ (See S.I. for details).

As shown in Figure 2(C), the oxidation wave of enamine was irreversible at low scan rates (< 1 V.s⁻¹). In order to provide evidence for the possible reduction of the electrogenerated enaminy radical species, the scan rate was increased to 400 V/s (corresponding to a time window of few ms), but the oxidation wave remained irreversible, indicating a very high instability of the generated species. In parallel, cyclic voltammetry experiments were also performed under full illumination of the solution, in order to photochemically generate enaminy radical cations. Here again, we could not capture the faradaic signature (reduction peak) of the enaminy radical cation, confirming the high reactivity/instability reported for these species.⁵⁸

**b) Observation of the enamine oxidation by the iridium complex excited state
(Reaction noted as 2 in Scheme 7)**

In order to determine whether the enamine species can be oxidized by the iridium complex excited state (*Ir), a Stern-Volmer dynamic/collisional quenching study was first attempted (see S.I.). As expected, the fluorescence intensity of *Ir decreased as the enamine concentration increased in agreement with a reaction between the fluorescent iridium excited state and enamine. Unfortunately, the uncertainty concerning the exact concentration of enamine in solution, the formation of which arising from a condensation equilibrium, precluded an accurate Stern-Volmer kinetic analysis. Instead, a known concentration of a stable commercially available enamine (1-pyrrolidino-1-cyclohexene) allowed a proper fluorescence quenching investigation (Figure 3).

In this case, a Stern-Volmer constant of 400 M^{-1} was found, a value that is of the same order of magnitude as the 200 M^{-1} that found by MacMillan for the quenching process involving a similar enamine and the excited state of $\text{Ir}(p\text{-MeO-ppy})_3$.⁴¹

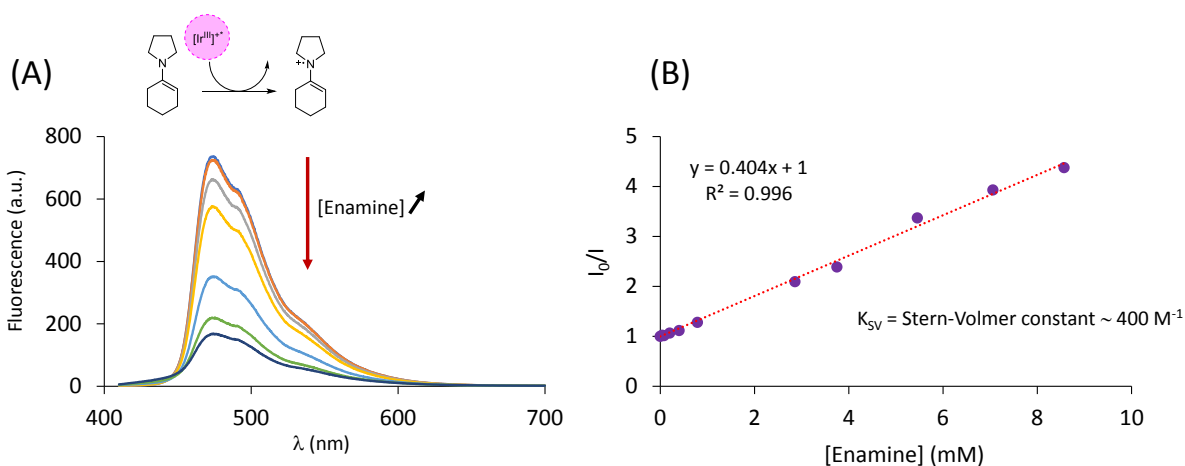


Figure 3. (A) Fluorescence collisional quenching between 1-pyrrolidino-1-cyclohexene and *Ir(III), and (B) corresponding Stern-Volmer kinetic analysis.

Alternatively, cyclic voltammetry can be used as an analytical tool to probe the enamine oxidation by the iridium complex excited state.

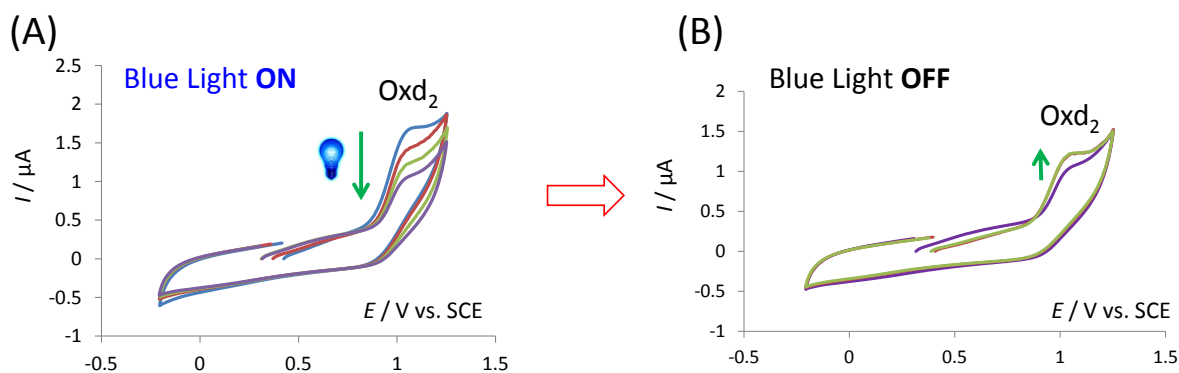


Figure 4. Electrochemical behavior of the *in-situ* formed enamine (wave Oxd₂) compound under blue illumination. Cyclic voltammograms performed at a GCE (1 mm in diameter) and at a scan rate of 100 mV/s in a DME/[TBA][BF₄] (0.3 M) solution containing Ir(dF(CF₃)ppy)₂(dtbbpy)](PF₆) (0.12 mM), *N*-methyl-trifluoroethanamine (17.6 mM), propanal (0.3 M), and *para*-toluenesulfonic acid (1.77 mM). Consecutive anodic scans performed under (A) blue light illumination then (B) after switching off the light.

As shown in Figure 4, running a series of cyclic voltammograms under blue light illumination led to a peak current intensity decrease of enamine (wave Oxd₂ in Figure 4(A)) accounting for a low and quasi stationary consumption of the enamine, which is generated by the condensation equilibrium and rapidly consumed by *Ir(III). Interestingly, the current intensity of Oxd₂ slightly increased after switching the light off (Figure 4(B)) indicating the return to the chemically-controlled enamine formation.

Contrary to cyclic voltammetry, which only perturbs a few micrometers layer of solution in the vicinity of the working electrode (the diffusion layer), photoexcitation (blue light illumination) affects the whole solution (the bulk), thus making transient local electrochemical techniques inadequate for more global investigations. Then, we decided to combine chronoamperometry (i.e. the monitoring of the current intensity with time) with a rotating disk electrode (RDE) to

ensure a stationary mass transport regime at the electrode surface (i.e., steady-state conditions). Under these conditions, the potential of the electrode was set at a sufficiently positive value (i.e., + 1 V), so that the enamine oxidation current was only limited by its transfer to the electrode and was directly proportional to its concentration in the solution. Note that the electrochemical behavior of enamine was the same at a GCE or platinum electrode.

Typical chronoamperometry traces are shown in Figure 5(A).

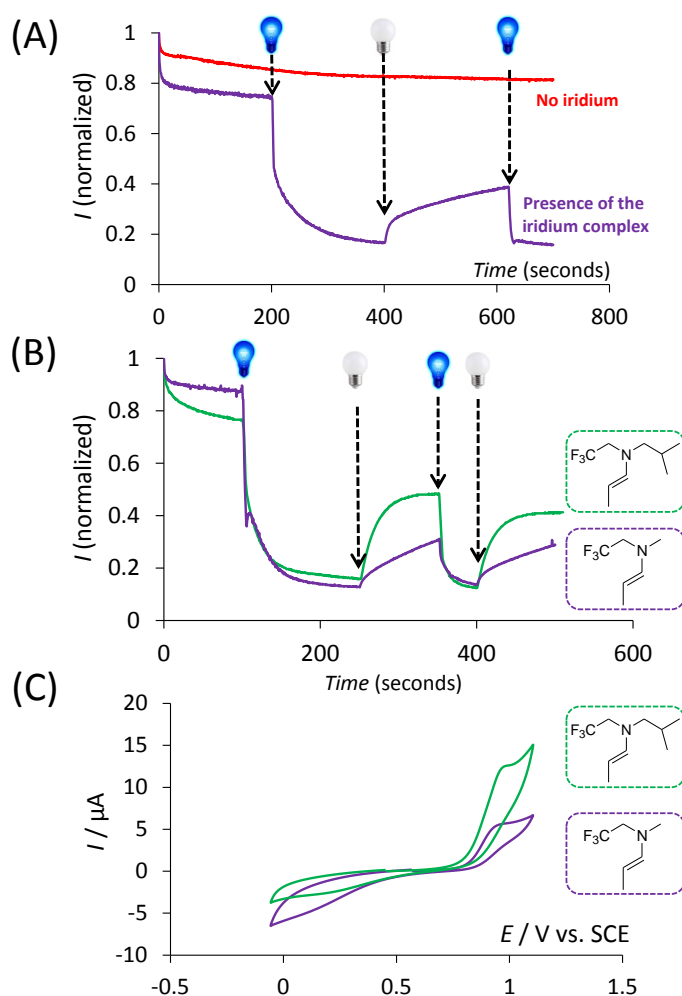


Figure 5. (A) Typical chronoamperograms obtained at a rotating platinum (2 mm in diameter) disk electrode (rotation rate: 2000 rpm) polarized at + 1 V/SCE and from DME/[TBA][BF₄] (0.3 M) solutions containing *N*-methyl-trifluoroethanamine (17.6 mM), propanal (0.3 M), and *para*-toluenesulfonic acid (3.5 mM). Chronoamperometry was performed in either the absence (red trace) or the presence (purple trace) of Ir(dF(CF₃)ppy)₂(dtbbpy)](PF₆) (0.37 mM).

(B) Chronoamperograms obtained under blue illumination, or not, for two different enamines formed *in-situ* from either (purple) *N*-methyl-trifluoroethanamine (17.6 mM) or (green) *N*-isobutyl-trifluoroethanamine (17.6 mM) in DME/[TBA][BF₄] (0.3 M) solutions containing propanal (0.3 M), *para*-toluenesulfonic acid (4.12 mM), and Ir(dF(CF₃)ppy)₂(dtbbpy)](PF₆) (0.29 mM). Conditions: rotating platinum (2 mm in diameter) disk electrode (rotation rate: 2000 rpm) polarized at + 1 V/SCE.

(C) Cyclic voltammograms of two different enamines formed *in-situ* from either (purple) *N*-methyl-trifluoroethanamine (17.6 mM) or (green) *N*-isobutyl-trifluoroethanamine (17.6 mM) in DME/[TBA][BF₄] (0.3 M) solutions containing propanal (0.3 M) and *para*-toluenesulfonic acid (4.3 mM).

In the absence of iridium, illumination of the solution had no influence on the consumption of enamine in solution in agreement with a quasi-stationary chronoamperogram (red trace in Figure 5(A)). However, when the iridium complex was present in solution, the blue LED illumination had a dramatic effect on the enamine consumption. Typically, a huge current decrease was observed as soon as the light was switched on indicating a consumption of the enamine in solution much faster than its formation from condensation of the amine and the aldehyde (purple trace in Figure 5(A)). In other words, the oxidation of enamine by the iridium photoexcited complex was so efficient that enamine formation could no longer fast enough to "replenish" the medium with enamine. Actually, the residual current represents that low quasi-stationary concentration of enamine remaining under illumination.

Importantly, stopping the illumination allowed the reformation of a stable amount of enamine, in agreement with the observed current increase. However, the current did not go back to its initial value (i.e., before lighting) showing that starting reagents responsible for the enamine formation (the aldehyde and/or the amine) have been consumed.

To confirm the robustness of chronoamperometry to monitor the concentration of the enamine intermediate, similar experiments were performed with another amine compound (*N*-isobutyl-

trifluoroethanamine). Compared to *N*-methyl-trifluoroethanamine, a similar current response was obtained under illumination and after switching off the light (green trace in Figure 5(B)). Nevertheless, the enamine reformation (through the chemical equilibrium 1 in Scheme 7) was faster and stronger with the isobutyl derivative in agreement with a higher current increase after turning off the illumination. This indicates that the condensation equilibrium constant was higher with the isobutyl amine derivative. Besides, comparison of cyclic voltammograms obtained under the same conditions by mixing propanal with either *N*-methyl-trifluoroethanamine or *N*-isobutyl-trifluoroethanamine clearly showed a higher peak current intensity with the latter in agreement with a more favorable displacement of the condensation equilibrium towards the enamine formation (Figure 5(C)).

4) Reactivity of the photo-generated electroactive enaminy radical species

In order to further explore the mechanism, the reactivity of the photo-generated enaminy radical cation was studied in the presence of either β -pinene or 2,4,6-tritertbutylbenzenthioi (ArSH , H-atom donor in the HAT cycle), or both compounds, by chronoamperometry at a rotating disk electrode.

a) Reactivity in the presence of beta-pinene (Reaction noted as 3 in Scheme 7)

The cyclic voltammogram of β -pinene exhibited an oxidation wave starting at around + 1.3 V with a peak located at ca. +1.5 V suggesting a slow electron transfer process. Moreover, and as shown in Figure 6(A), this oxidation wave totally disappeared after a consecutive second run showing a strong passivation of the electrode surface by β -pinene. Besides, polishing the electrode surface was sufficient to recover the β -pinene oxidation wave.

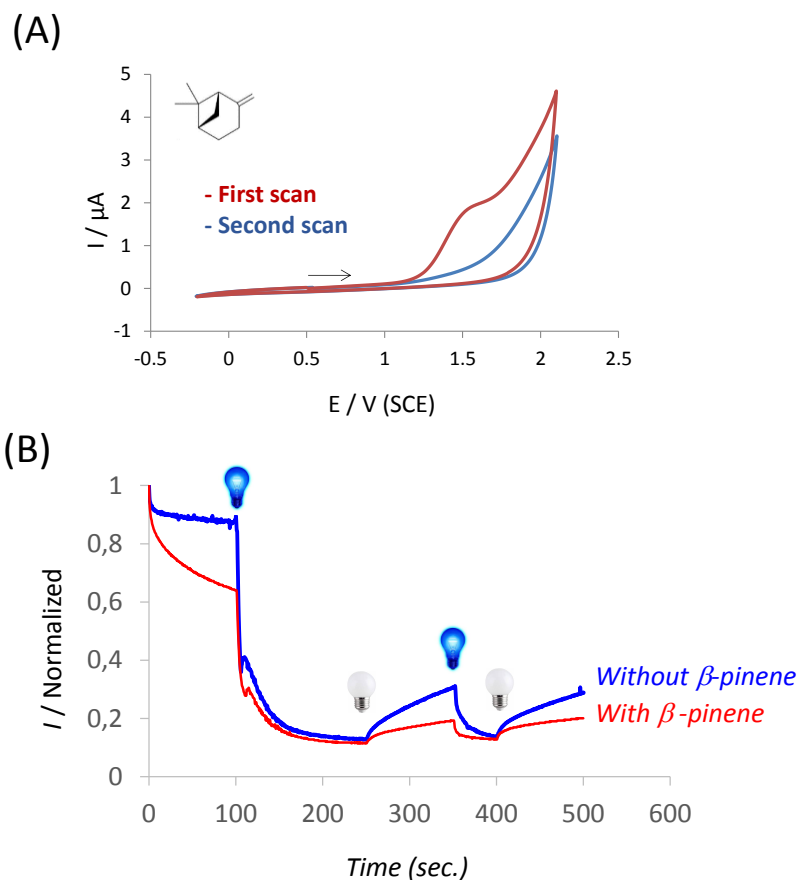


Figure 6. (A) Cyclic voltammograms of β -pinene (20 mM), in DME/[TBA][BF₄] (0.3 M), at a platinum electrode (0.5 mm in diameter), and at a scan rate of 100 mV/s. First scan in red and second scan in blue. (B) Chronoamperograms obtained in (blue) the absence or (red) the presence of β -pinene (0.25 M). Conditions: DME/[TBA][BF₄] (0.3 M), *N*-methyltrifluoroethanamine (17.6 mM), propanal (0.3 M), *para*-toluenesulfonic acid (4.24 mM), Ir(dF(CF₃)ppy)₂(dtbbpy)](PF₆) (0.28 mM); platinum rotating (2 mm in diameter) disk electrode (rotation rate: 2000 rpm) polarized at + 1 V/SCE.

Chronoamperometric investigations were performed under illumination, or not, in the absence or presence of β -pinene at a sufficiently positive potential value (+ 1 V) to oxidize the enamine (Figure 6(B)). During the first 100 seconds, the current value corresponding to the enamine oxidation decreased faster in the presence of β -pinene despite the fact that the light was switched off. Actually, this behavior is consistent with the adsorption of β -pinene at the electrode surface

observed during cyclic voltammetry experiments. Under illumination, a rapid current decrease was observed not only in the absence, but also in the presence of β -pinene with a residual current of the same magnitude as the one obtained in the absence of β -pinene, suggesting that adsorption no longer occurred under illumination. Then, switching off the light led to a current increase that was higher in the absence than in the presence of β -pinene (compare the blue and red traces in Figure 6(B)). At this stage, it is difficult to know whether this difference comes from a higher depletion of the enamine in the diffusion layer ascribed to a reaction between the enaminy radical species and β -pinene or a passivation of the electrode surface by the latter species.

b) Reactivity in the presence of ArSH (triisopropylbenzenethiol)

In parallel, the possible (late) reactivity of the photo-generated enaminy radical species towards triisopropylbenzenethiol (ArSH) was also tested. First, cyclic voltammetry experiments were performed to determine the redox potential values of crucial species such as ArSH, ArS[•] or ArS⁻ that are involved in the HAT catalytic cycle.

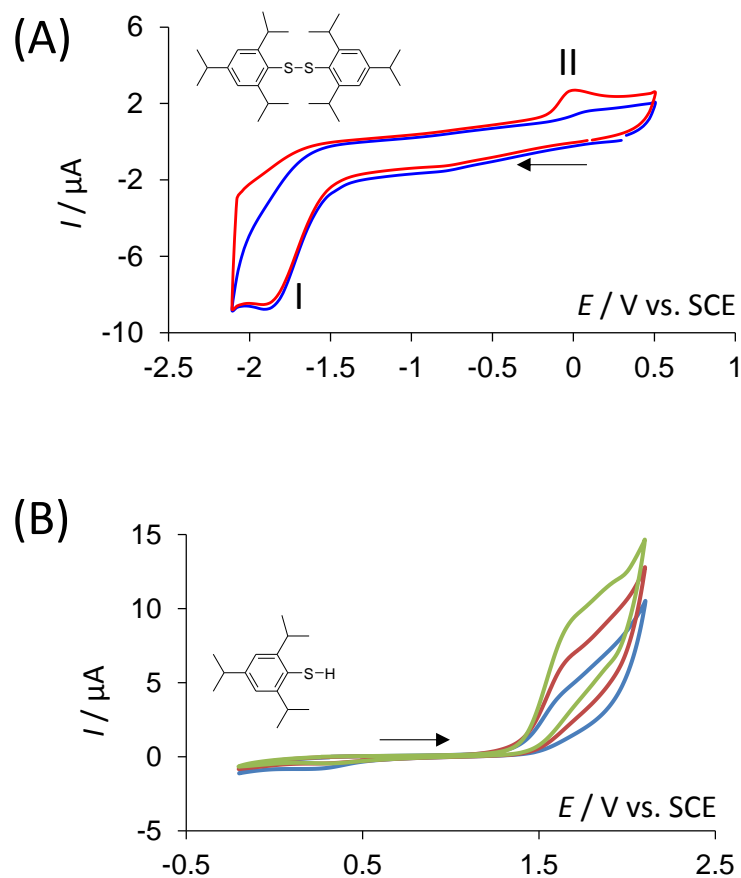
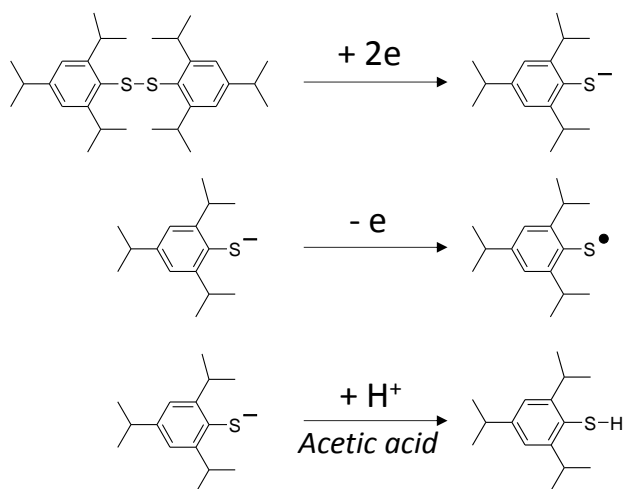


Figure 7. (A) Cyclic voltammograms of bis(2,4,6-triisopropylphenyl) disulfide (1.19 mM) performed in DME/[TBA][BF₄] (0.3 M), at a glassy carbon electrode (1 mm in diameter), and at a scan rate of 200 mV/s, by maintaining (red curve), or not (blue curve), the potential at a constant value of -2.1 V for 15 seconds. (B) Cyclic voltammograms of tri-isopropylbenzenethiol (3.4 mM (a), 6.8 mM (b), 10.2 mM (c)) performed in DME/[TBA][BF₄] (0.3 M), at a platinum electrode (0.5 mm in diameter), and at a scan rate of 100 mV/s.

The 2,4,6-triisopropylphenylsulfide anion was generated by electrochemical reduction (wave I at -1.9 V) of the corresponding disulfide compound (Figure 7(A)).⁵⁹⁻⁶² The latter were then oxidized at +0.01 V (wave II in Figure 7(A)) during the backward potential scan. Holding the potential value at -2.1 V for about 15 seconds allowed generation of a larger amount of anions at the electrode surface and to increase their oxidation wave II. Interestingly, the addition of acetic acid (5 μL ; pK_a = 4.8) led to the disappearance of wave noted II in Figure 7(A) in

agreement with a protonation of anions (Scheme 5). Importantly, the presence of water had no effect on the oxidation wave II demonstrating that anions were not protonated under these conditions.



Scheme 5. Mechanistic scheme of the reduction of bis(2,4,6-triisopropylphenyl) disulfide in the absence or the presence of acid.

Unfortunately, this oxidation wave II (Figure 7(A)) remained irreversible even at several hundred volts per second preventing thus the observation of the reduction wave of the ArS^{\bullet} as well as the access to the standard potential value of the $\text{ArS}^{\bullet} / \text{ArS}^{\bullet-}$ redox couple. However, on the basis of the work described by Savéant about the dependence of the standard potential E° of the $\text{PhS}^{\bullet} / \text{PhS}^{\bullet-}$ couple with the electronic effects of the substituents (associated to the Hammett constant) carried by the phenyl ring⁶³ a value of + 0.01 V for the $\text{ArS}^{\bullet} / \text{ArS}^{\bullet-}$ redox couple under our conditions is really consistent.

Finally, it was also relevant to investigate the electrochemical behavior of triisopropylbenzenethiol (ArSH) which is supposed to trigger the HAT cycle (Scheme 1). Under these conditions, and as shown in Figure 7(B), the reduction of ArSH occurred at around +1.65

V. This compound is thus more difficult to oxidize than the enamine (+1 V) and somewhat easier to oxidize than the starting amine (+1.75 V). Moreover, the presence of this oxidation wave indicated that ArSH was not in its basic form in DME.

Chronoamperometric investigations were then performed in the presence of the *in-situ* formed enamine and ArSH (Figure 8). As previously observed in the presence of β -pinene, a current decrease is observed in the absence of illumination also suggesting a fouling of the electrode surface by the enamine itself. Nevertheless, assuming a similar electrode passivation in the absence and presence of ArSH (compare curve (a) and (b) in Figure 8), illumination of the solution caused a fast consumption of enamine upon several seconds that was slightly slower in the presence of ArSH (red trace in Figure 8).

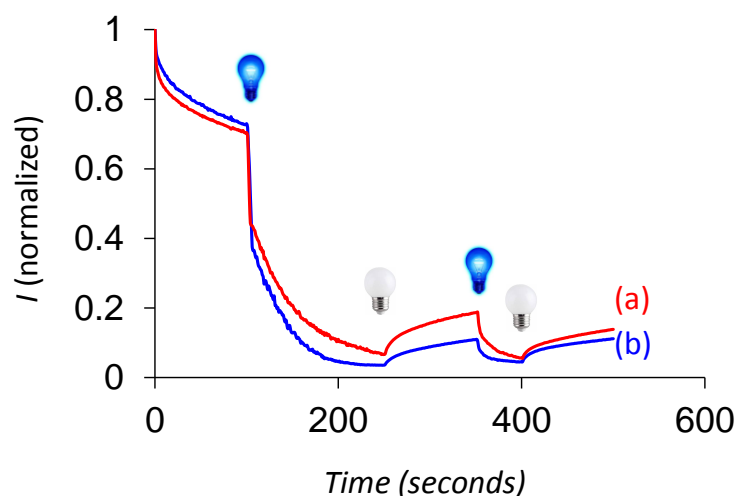
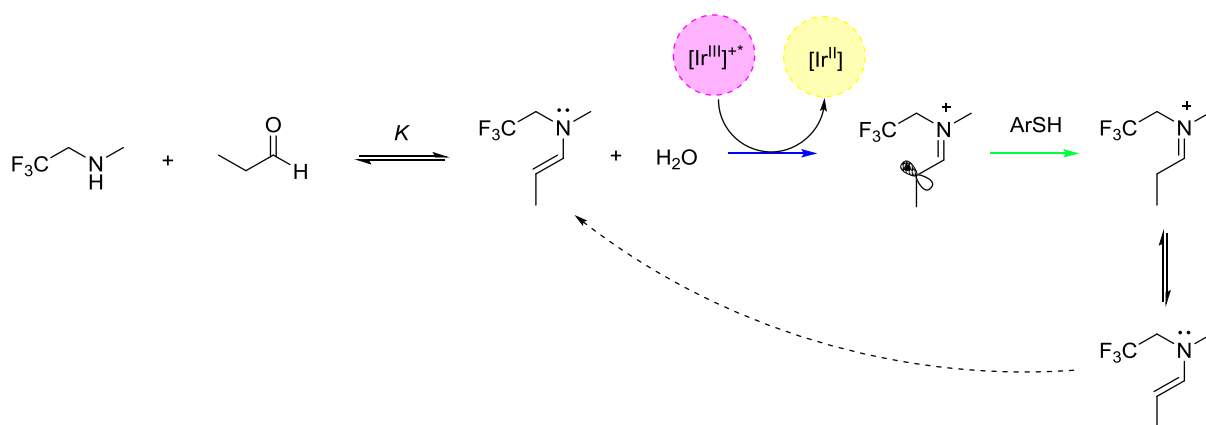


Figure 8. Chronoamperograms obtained in (red (a)) the presence or the absence (blue (b)) of triisopropylbenzenethiol (ArSH) (6 mM). Conditions: DME/[TBA][BF₄] (0.3 M), *N*-methyltrifluoroethanamine (17.6 mM), propanal (0.3 M), *para*-toluenesulfonic acid (2.3 mM), Ir(dF(CF₃)ppy)₂(dtbbpy)](PF₆) (0.18 mM); platinum rotating (2 mm in diameter) disk electrode (rotation rate: 2000 rpm) polarized at +1 V/SCE.

Since ArSH is not expected to directly react with the enamine, this behavior most likely accounts for a better regeneration of the enamine in the presence of ArSH. This is consistent with a H atom abstraction step leading to the corresponding enaminy radical species. The latter would be then reduced by Ir(II) coming from the reductive quenching of $^*Ir(III)$ with regenerating thus the enamine derivative as well as the Ir(III) complex (Scheme 6). Accordingly, after stopping the illumination at 250 seconds, the current increase was more pronounced in the presence of ArSH since a significant part of enamine would have been regenerated.



Scheme 6. Proposed mechanism for the regeneration of enamine in the presence of ArSH without β -pinene.

c) Reactivity in the presence of both β -pinene and ArSH (Reactions 3 + 4 in Scheme 7)

Finally, the reactivity of the photo-generated enaminy radical species was investigated in the presence of both β -pinene and ArSH and compared to similar experiments carried out in the absence of ArSH (Figure 9).

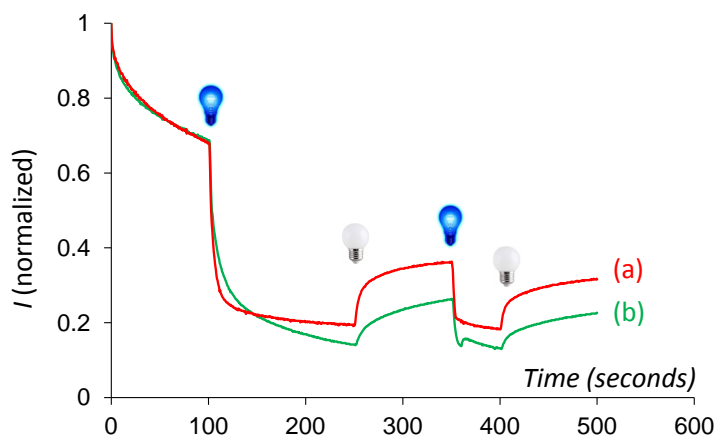


Figure 9. Chronoamperograms obtained in (red (a)) the presence or the absence (green (b)) of triisopropylbenzenethiol (ArSH) (6 mM). Conditions: DME/[TBA][BF₄] (0.3 M), *N*-methyltrifluoroethanamine (17.6 mM), propanal (0.3 M), *para*-toluenesulfonic acid (2.3 mM), β -pinene (0.3 M), Ir(dF(CF₃)ppy)₂(dtbbpy)](PF₆) (0.18 mM); platinum rotating (2 mm in diameter) disk electrode (rotation rate: 2000 rpm) polarized at + 1 V/SCE.

Here again, chronoamperometric investigations focus on the enamine oxidation current (potential value set at + 1 V) which is a central species to monitor the catalytic process in real time. Interestingly, and assuming a similar electrode passivation in the absence or the presence of ArSH (see between $0 < t < 100$ sec.), the enamine consumption/regeneration followed two distinct behaviors (Figure 9): Under illumination ($100 < t < 250$ sec), the current intensity reached a plateau when ArSH was present in the solution, but continued to decrease in the absence of the thiol derivative. Assuming only β -pinene reacts on the enaminy radical cation, this behavior would provide evidence that the stationary regeneration of the enamine is ArSH-dependent, but via an indirect mechanism different than that described in Scheme 6. Actually, considering the redox potential values of species such as ArSH, ArS[•] or ArS⁻, the occurrence of a HAT cycle appears consistent with the amine regeneration as well as the ultimate formation of the coupling product.

Furthermore, gas chromatography analyses performed after 10 minutes of illumination on solutions similar to those described in Figure 9 established that a tenfold increase in the amount of coupling product was obtained in the presence of ArSH. The enamine oxidation current intensity being also higher in the presence of ArSH (See S.I.), the enamine regenerative property of the overall light-mediated process (i.e. its catalytic nature) is established.

At this stage, it is also important to note that redox potential values of the $[\text{Ir}^{\text{III}}]^+ / \text{Ir}^{\text{II}}$ and the $\text{ArS}^\bullet / \text{ArS}^-$ couples ($E^\circ = -1.12$ and $+0.01$ V, respectively) make a redox reaction between Ir^{II} and ArS^\bullet favorable to regenerate $[\text{Ir}^{\text{III}}]^+$ and ArS^- , allowing completion of the photocatalytic and HAT cycles (Scheme 7). The full catalytic sequence may therefore be depicted with a more explicit interaction and inter-dependence between both processes.

Finally, it was interesting to verify the possible role of water on the coupling product formation as well as on the amine/enamine regeneration. According to the mechanism proposed by MacMillan the presence of water molecules is required to produce the coupling product and to regenerate the amine organocatalyst during the last step (reaction noted as 5 in Scheme 7).

As previously experimented with ArSH, two independent analyses were performed. First an electroanalysis by chronoamperometry, then a GC analysis of solutions illuminated for 10 minutes to check the distribution of products (preparative way; see S.I for the corresponding chronoamperometric traces).

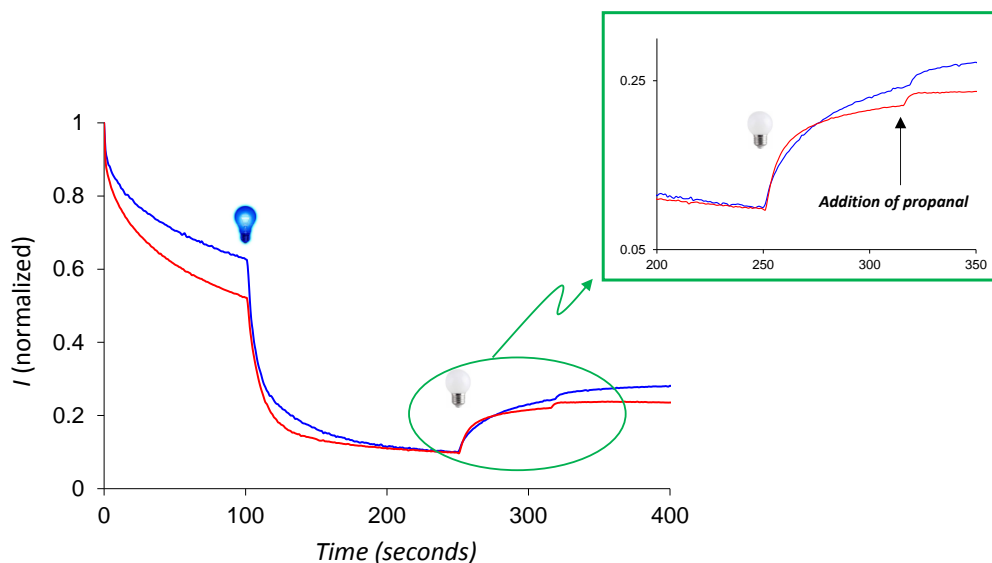


Figure 10. Red trace: Chronoamperogram obtained at a platinum rotating (2 mm in diameter) disk electrode (rotation rate: 2000 rpm) polarized at + 1 V/SCE, in a DME/[TBA][BF₄] (0.3 M) solution containing *N*-methyl-trifluoroethanamine (17.6 mM), propanal (0.3 M), *para*-toluenesulfonic acid (2.1 mM), β -pinene (0.3 M), tri-isopropylbenzenethiol (ArSH - 6 mM), water (88.8 mM), and Ir(dF(CF₃)ppy)₂(dtbbpy)](PF₆) (0.18 mM). Blue trace: same conditions than the red trace, but without water. In both cases, propanal (105.6 μ L) was added at 310 seconds. The inset is a zoom for 200 < t < 350 seconds.

In Figure 10 are shown two chronoamperometric investigations performed in the absence or the presence of water. In the absence of blue light ($t < 100$ s), the current ascribed to the enamine oxidation decreased faster in the presence of water (red trace). Assuming that water does not foul the electrode surface and considering the condensation equilibrium, this behavior would be in agreement with the fact that water disfavors the enamine formation equilibrium (reaction noted as 1 in Scheme 7). However, under illumination, the current evolution was very similar in the presence or the absence of water. In both cases, a similar plateau current was reached (in agreement with the presence of ArSH), but no significant effect on enamine oxidation current (and hence regeneration) was observed. Actually, a slight effect could be observed during the first seconds after switching off the light in agreement with a faster current increase in the presence of water (see the inset in Figure 10). At longer timescales, the enamine regeneration

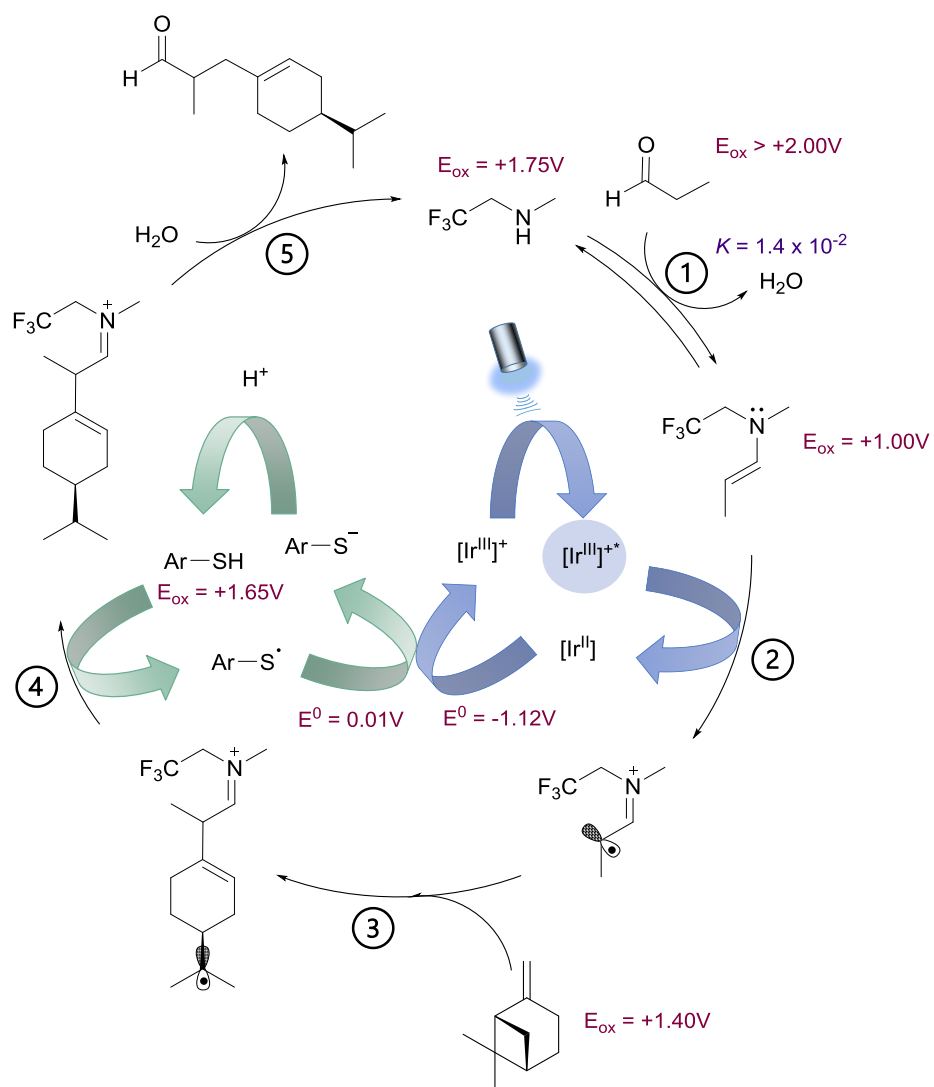
became more efficient in the absence of water, mostly accounting for the unfavorable displacement of the condensation equilibrium. Accordingly, the addition of propanal (in both cases) led to a current increase in agreement with a *Le Chatelier* effect on the equilibrium governing the enamine formation (reaction noted as 1 in Scheme 7).

Similarly, GC analysis of solutions illuminated for 10 minutes (preparative way – see the chronoamperogram in S.I.) did not show a higher production of the coupling product in the presence of water. Conversely, in the presence of water (8 μL) the coupling product was produced with a slightly lower yield compared to the experiment carried out in the absence of water. Under our conditions (excess of water), the addition of water would actually mainly affect the enamine formation. Actually, i) the enamine formation equilibrium is sufficiently fast and ii) the amount of water molecule liberated by the condensation reaction are very likely sufficient to allow completion of the organocatalytic cycle.

CONCLUSION

This work was aimed at implementing electrochemical methods to monitor the evolution and fate of electroactive species in a complex organocatalytic/photocatalytic/HAT sequence. The mechanism consisted in a light-promoted coupling of propanal with β -pinene, featuring an electroactive enamine intermediate. Cyclic voltammetry allowed the determination of the oxidation and reduction potential values of several actors of the catalytic process (iridium photoactivable complex, amines, thiols). However, such thermodynamic data remain “static” information on the possible electron transfers taking place in the medium, providing at best a frozen framework of the possible reactions. The in-situ chronoamperometric monitoring of the

concentration of the enamine under various constraints (light on or off, absence/presence of other substrates or quenchers) has highlighted both the effects of the concentration of the reactants and products on the condensation equilibrium and the regenerative (catalytic) nature of the overall process. In other words, chronoamperometry enables a dynamic characterization of the catalytic process. Therefore, electrochemical approaches, through the monitoring of even a single electroactive intermediate, introduce a key analytical tool providing an overview of the catalytic sequence under operando conditions. Accordingly, the general triple catalytic sequence proposed by MacMillan for the coupling of aldehydes with olefins has been confirmed and its chronology strengthened. In this context, it was notably demonstrated the inter-dependence between the photocatalytic and HAT processes (Scheme 7). Undoubtedly, the focus on one or more electroactive intermediates in a photoredox catalytic sequence allows a real time follow-up of the concentration of these species during the reaction, thus confirming or completing the information collected by other approaches.



Scheme 7. Comprehensive mechanistic framework of the blue light-mediated coupling of propanal with β -pinene highlighting the steps (1-5) assessed by our electrochemical approach

AUTHOR INFORMATION

Corresponding Authors

* **Julie Quintaine.** Discovery chemistry & Development, Research & Development, dsm-firmenich, 7 rue de la Bergère, CH-1242 Satigny, Geneva, Switzerland.

Email: Julie.Quintaine@firmenich.com

* **Olivier Buriez.** PASTEUR, Département de Chimie, Ecole Normale Supérieure, PSL University, Sorbonne Université, CNRS, 75005 Paris, France.

ORCID : 0000-0001-5452-1942 ; Email : olivier.buriez@ens.psl.eu

Author Contributions

The manuscript was written through contributions of all authors. All authors have given approval to the final version of the manuscript. ‡These authors contributed equally.

Notes

The authors declare no competing financial interest.

ASSOCIATED CONTENT

Supporting Information. Absorption and fluorescence spectra of the iridium complex; Estimation of the enamine formation constant; Stern-Volmer dynamic/collisional quenching study; Fluorescence collisional quenching between the *in-situ* formed enamine species and the iridium complex excited state; Chronoamperograms obtained in view of gas chromatography analyses;

ACKNOWLEDGMENT

Research reported in this publication was supported by dsm-firmenich, CNRS UMR 8640, Ecole Normale Supérieure, PSL University, and Sorbonne Université. The authors would like to thank Dr T. Le Saux for performing the absorption and fluorescence spectra of the iridium complex.

REFERENCES

- (1) Prier, C. K.; Rankic, D. A.; MacMillan, D. W. C. Visible Light Photoredox Catalysis with Transition Metal Complexes: Applications in Organic Synthesis. *Chem. Rev.* **2013**, *113*, 5322–5363.
- (2) Xi, Y.; Yi, H.; Lei, A. Synthetic Applications of Photoredox Catalysis with Visible Light. *Org. Biomol. Chem.* **2013**, *11*, 2387–2403.
- (3) Xuan, J.; Xiao, W.-J. Visible-Light Photoredox Catalysis. *Angew. Chem., Int. Ed.* **2012**, *51*, 6828–6838.
- (4) Tucker, J. W.; Stephenson, C. R. J. Shining Light on Photoredox Catalysis: Theory and Synthetic Applications. *J. Org. Chem.* **2012**, *77*, 1617–1622.
- (5) Ischay, M. A.; Yoon, T. P. Accessing the Synthetic Chemistry of Radical Ions. *Eur. J. Org. Chem.* **2012**, *2012*, 3359–3372.
- (6) Reckenthäler, M.; Griesbeck, A. G. Photoredox Catalysis for Organic Syntheses. *Adv. Synth. Catal.* **2013**, *355*, 2727–2744.
- (7) Narayanam, J. M. R.; Stephenson, C. R. J. Visible Light Photoredox Catalysis: Applications in Organic Synthesis. *Chem. Soc. Rev.* **2011**, *40*, 102.

- (8) N. A. Romero, D. A. Nicewicz. Organic Photoredox Catalysis. *Chem. Rev.* **2016**, *116*, 10075–10166.
- (9) Arias-Rotondo, D. M.; McCusker, J. K. The Photophysics of Photoredox Catalysis: A Roadmap for Catalyst Design. *Chem. Soc. Rev.* **2016**, *45*, 5803–5820.
- (10) Pitre, S. P.; McTiernan, C. D.; Scaiano, J. C. Understanding the Kinetics and Spectroscopy of Photoredox Catalysis and Transition-Metal-Free Alternatives. *Acc. Chem. Res.* **2016**, *49*, 1320–1330.
- (11) Blanksby, S. J.; Ellison, G. B. Bond Dissociation Energies of Organic Molecules. *Acc. Chem. Res.* **2003**, *36*, 255–263.
- (12) Waidmann, C. R.; Miller, A. J. M.; Ng, C.-W. A.; Scheuermann, M. L.; Porter, T. R.; Tronic, T. A.; Mayer, J. M. Using Combinations of Oxidants and Bases as PCET Reactants: Thermochemical and Practical Considerations. *Energy Environ. Sci.* **2012**, *5*, 7771–7780.
- (13) Koyama, D.; Dale, D. J. A.; Orr-Ewing, A. J. Ultrafast Observation of a Photoredox Reaction Mechanism: Photoinitiation in Organocatalyzed Atom-Transfer Radical Polymerization. *J. Am. Chem. Soc.* **2018**, *140*, 1285–1293.
- (14) Lewis-Borrell, L.; Sneha, M.; Bhattacharjee, A.; Clark, I. P.; Orr-Ewing, A. J. Mapping the Multi-step Mechanism of a Photoredox Catalyzed Atom-Transfer Radical Polymerization Reaction by Direct Observation of the Reactive Intermediates. *Chem. Sci.* **2020**, *11*, 4475–4481.
- (15) Romero, N. A.; Nicewicz, D. A. Mechanistic Insight into the Photoredox Catalysis of Anti-Markovnikov Alkene Hydrofunctionalization Reactions. *J. Am. Chem. Soc.* **2014**, *136*, 17024–17035.

- (16) Ruccolo, S.; Qin, Y.; Schnedermann, C.; Nocera, D. G. General Strategy for Improving the Quantum Efficiency of Photoredox Hydroamidation Catalysis. *J. Am. Chem. Soc.* **2018**, *140*, 14926–14937.
- (17) Martinez-Haya, R.; Miranda, M. A.; Marin, M. L. Metal-Free Photocatalytic Reductive Dehalogenation Using Visible-Light: A Time-Resolved Mechanistic Study. *Eur. J. Org. Chem.* **2017**, *2017*, 2164–2169.
- (18) Herzog, W.; Bronner, C.; Löffler, S.; He, B.; Kratzert, D.; Stalke, D.; Hauser, A.; Wenger, O. S. Electron Transfer between Hydrogen-Bonded Pyridylphenols and a Photoexcited Rhenium(I) Complex. *ChemPhysChem.* **2013**, *14*, 1168–1176.
- (19) Rueda-Becerril, M.; Mahé, O.; Drouin, M.; Majewski, M. B.; West, J. G.; Wolf, M. O.; Sammis, G. M.; Paquin, J.-F. Direct C–F Bond Formation Using Photoredox Catalysis. *J. Am. Chem. Soc.* **2014**, *136*, 2637–2641.
- (20) Majek, M.; Jacobi von Wangelin, A. Mechanistic Perspectives on Organic Photoredox Catalysis for Aromatic Substitutions. *Acc. Chem. Res.* **2016**, *49*, 2316–2327.
- (21) Ng, Y. Y.; Tan, L. J.; Ng, S. M.; Chai, Y. T.; Ganguly, R.; Du, Y.; Yeow, E. K. L.; Soo, H. S. Spectroscopic Characterization and Mechanistic Studies on Visible Light Photoredox Carbon-Carbon Bond Formation by Bis(Arylimino)Acenaphthene Copper Photosensitizers. *ACS Catal.* **2018**, *8*, 11277–11286.
- (22) Ma, J.; Zhang, X.; Phillips, D. L. Time-Resolved Spectroscopic Observation and Characterization of Water-Assisted Photoredox Reactions of Selected Aromatic Carbonyl Compounds. *Acc. Chem. Res.* **2019**, *52*, 726–737.

- (23) Ting, S. I.; Garakyaraghi, S.; Taliaferro, C. M.; Shields, B. J.; Scholes, G. D.; Castellano, F. N.; Doyle, A. G. 3d-d Excited States of Ni(II) Complexes Relevant to Photoredox Catalysis: Spectroscopic Identification and Mechanistic Implications. *J. Am. Chem. Soc.* **2020**, *142*, 5800–5810.
- (24) Zheng, S.; Zhang, S.-Q.; Saeednia, B.; Zhou, J.; Anna, J. M.; Hong, X.; Molander, G. A. Diastereoselective Olefin Amidoacylation via Photoredox PCET/Nickel-Dual Catalysis: Reaction Scope and Mechanistic Insights. *Chem. Sci.* **2020**, *11*, 4131–4137.
- (25) Coles, M. S.; Quach, G.; Beves, J. E.; Moore, E. G. A Photophysical Study of the Sensitization-Initiated Electron Transfer: Insights into the Mechanism of Photoredox Activity. *Angew. Chem., Int. Ed.* **2020**, *59*, 9522–9526.
- (26) Wang, K.; Lu, H.; Zhu, X.; Lin, Y.; Beard, M. C.; Yan, Y.; Chen, X. Ultrafast Reaction Mechanisms in Perovskite Based Photocatalytic C-C Coupling. *ACS Energy Lett.* **2020**, *5*, 566–571.
- (27) Stevenson, B.G.; Spielvogel, E. H.; Loiaconi, E. A.; Wambua, V. M.; Nakhmiyayev, R. V.; Swierk, J. R. Mechanistic Investigations of an α -Aminoarylation Photoredox Reaction. *J. Am. Chem. Soc.* **2021**, *143*, 8878–8885.
- (28) McNally, A.; Prier, C. K.; MacMillan, D. W. C. Discovery of an α -Amino C–H Arylation Reaction Using the Strategy of Accelerated Serendipity. *Science*. **2011**, *334*, 1114–1117.
- (29) Spielvogel, E. H.; Stevenson, B. G.; Stringer, M. J.; Hu, Y.; Fredin, L. A.; Swierk, J. R. Insights into the Mechanism of an Allylic Arylation Reaction via Photoredox-Coupled Hydrogen Atom Transfer. *J. Org. Chem.* **2022**, *87*, 223–230.

- (30) Cuthbertson, J. D.; MacMillan, D. W. The direct arylation of allylic sp³ C–H bonds via organic and photoredox catalysis. *Nature*. **2015**, *519*, 74–77.
- (31) Jutand, A. Contribution of Electrochemistry to Organometallic Catalysis. *Chem. Rev.* **2008**, *108*, 7, 2300–2347.
- (32) McKenzie, E. C. R.; Hosseini, S.; Petro, A. G. C.; Rudman, K. K.; Gerroll, B. H. R.; Mubarak, M. S.; Baker, L. A.; Little, R. D. Versatile Tools for Understanding Electrosynthetic Mechanisms. *Chem. Rev.* **2022**, *122*, 3292–3335.
- (33) Labbé, E.; Buriez, O. Fundamental Input of Analytical Electrochemistry in the Determination of Intermediates and Reaction Mechanisms in Electrosynthetic Processes. *ChemElectroChem*. **2019**, *6*, 4118-4125.
- (34) Buriez, O.; Labbé, E. Disclosing the redox metabolism of drugs: The essential role of electrochemistry. *Current Opinion in Electrochemistry*. **2020**, *24*, 63-68.
- (35) Amatore, C.; Labbé, E.; Buriez, O. Molecular electrochemistry: A central method to understand the metabolic activation of therapeutic agents. The example of metallocifen anti-cancer drug candidates. *Current Opinion in Electrochemistry*. **2017**, *2*, 7-12.
- (36) Bonometti, V.; Labbé, E.; Buriez, O.; Mussini, P.; Amatore, C. Exploring the first steps of an electrochemically-triggered controlled polymerization sequence: Activation of alkyl- and benzyl halide initiators by an electrogenerated FeII-Salen complex. *J. Electroanal. Chem.* **2009**, *633*, 99-105.

- (37) Enders, P.; Májek, M.; Lam, C. M.; Little, R. D.; Francke, R. How to Harness Electrochemical Mediators for Photocatalysis – A Systematic Approach Using the Phenanthro[9,10-*d*]imidazole Framework as a Test Case. *ChemCatChem*. **2023**, *15*, e202200830.
- (38) Shaw, N. H.; Twilton, J.; MacMillan, D. W. C. Photoredox Catalysis in Organic Chemistry. *J. Org. Chem.* **2016**, *81*, 6898–6926.
- (39) Lipp, A.; Badir, S. O.; Molander, G. A. Stereoinduction in Metallaphotoredox Catalysis. *Angew. Chem. Int. Ed.* **2021**, *60*, 1714–1726.
- (40) Pirnot, M. T.; Rankic, D. A.; Martin, D. B. C.; MacMillan, D. W. C. Photoredox Activation for the Direct β -Arylation of Ketones and Aldehydes. *Science* **2013**, *339*, 1593–1596.
- (41) Petronijević, F. R. ; Nappi, M. ; MacMillan, D. W. C. Direct β -Functionalization of Cyclic Ketones with Aryl Ketones via the Merger of Photoredox and Organocatalysis. *J. Am. Chem. Soc.* **2013**, *135*, 18323–18326.
- (42) Jeffrey, J. L. ; Petronijević, F. R. ; MacMillan, D. W. C. Selective Radical–Radical Cross Couplings: Design of a Formal β -Mannich Reaction. *J. Am. Chem. Soc.* **2015**, *137*, 8404–8407.
- (43) Terrett, J. A.; Clift, M. D.; MacMillan, D. W. C. Direct β -Alkylation of Aldehydes via Photoredox Organocatalysis. *J. Am. Chem. Soc.* **2014**, *136*, 6858–6861.
- (44) DeHovitz, J. S.; Loh, Y. Y.; Kautzky, J. A.; Nagao, K.; Meichan, A. J.; Yamauchi, M.; MacMillan, D. W. C.; Hyster, T. K. Static to inducibly dynamic stereocontrol: The convergent use of racemic β -substituted ketones. *Science* **2020**, *369*, 1113–1118.

- (45) Sombret, J. ; Quintaine, J. ; Biremond, T. ; Barnes, Q. ; de Saint-Laumer, J.-Y. ; Saudan, L. High trans-2-Decalones by Photoredox Catalyzed β -Isomerization. *Helv. Chim. Acta* **2022**, *105*, e202100180.
- (46) Capacci, A. G.; Malinowski, J. T.; McAlpine, N. J.; Kuhne, J.; MacMillan, D. W. C. Direct, enantioselective α -alkylation of aldehydes using simple olefins. *Nature Chemistry*. **2017**, *9*, 1073-1077.
- (47) Quintaine, J.; MacMillan, D. W. C. Alpha-alkylation of aldehyde with a polycyclic olefin. Patent WO2018/192923 (**2018**) to Firmenich SA.
- (48) Lowry, M. S.; Goldsmith, J. I.; Slinker, J. D.; Rohl, R.; Pascal, R. A.; Malliaras, Jr, G. G.; Bernhard, S. Single-layer electroluminescent devices and photoinduced hydrogen production from ionic iridium (III) complex. *Chem. Mater.* **2005**, *17*, 5712-5719.
- (49) Renard, M. ; Ghosez, L. A. A convergent asymmetric synthesis of gamma-butenolides. *Tetrahedron* **2001**, *57*, 2597-2608.
- (50) Umemoto, T.; Singh, R. P. Methods for preparing diaryl disulfides. Patent US2012/0157716 (**2012**) to Ube Industries, Ltd.
- (51) Bissell, E. R.; Finger, M. Fluorine-Containing Nitrogen Compounds. I. Trifluoroethylamines. *J. Org. Chem.* **1959**, *24*, 1256-1259.
- (52) Markwalder, J. A.; Seitz, S. P.; Balog, J. A.; Huang, A.; Williams, D. K.; Chen, L.; Mandal, S. K.; Srivastava, S. IDO inhibitors. Patent WO 2015/031295 (**2015**) to Bristol-Myers Squibb.
- (53) Knibbe, H.; Rehm, D.; Weller, A. Intermediates and Kinetics of Fluorescence Quenching by Electron Transfer. *Ber. Bunsen-Ges. Phys. Chem.* **1968**, *72*, 257-263.

- (54) Tay, N. E. S.; Lehnherr, D.; Rovis, T. Photons or Electrons? A Critical Comparison of Electrochemistry and Photoredox Catalysis for Organic Synthesis. *Chem. Rev.* **2022**, *122*, 2487–2649.
- (55) Bevernaegie, R.; Wehlin, S. A.M.; Elias, B.; Troian-Gautier, L. A Roadmap Towards Visible Light Mediated Electron Transfer Chemistry with Iridium(III) Complexes. *ChemPhotoChem.* **2021**, *5*, 217–234.
- (56) Amatore, C., Basic Concepts. In “Organic Electrochemistry” (4th Edition), Lund, H. and Hammerich, O., Ed. Marcel Dekker: New York, **2001**, 1-94.
- (57) Li, Y.; Wang, D.H.; Zhang, L.; Luo, S.Z. Redox Property of Enamines. *J. Org. Chem.* **2019**, *84*, 12071-12090.
- (58) Schoeller, W. W.; Niemann, J.; Rademacher, P. On the Electrochemical Oxidation of Enamines. *J. Chem. Soc. Perkin Trans. II.* **1988**, 369-373.
- (59) Maran, F.; Wayner, D.D.M.; Workentin, M.S. Kinetics and mechanism of the dissociative reduction of C-X and X-X bonds (X = O, S). *Advances in Physical Organic Chemistry*, **2001**, *36*, 85-166.
- (60) Christensen, T.B.; Daasbjerg, K. Investigation of the direct and indirect reduction processes of some disulfides by electrochemical means. *Acta Chemica Scandinavica*, **1997**, *51*, 307-317.
- (61) Arévalo, M.C.; Maran, F.; Severin, M.G.; Vianello, E. A case of the indirect role of traces of water in the electroreduction of organic substrates. *J. Electroanal. Chem.* **1996**, *418*, 47-52.

(62) Borsari, M.; Cannio, M.; Gavioli, G. Electrochemical behavior of diphenyl disulfide and thiophenol on glassy carbon and gold electrodes in aprotic media. *Electroanalysis*, **2003**, *15*, 1192-1197.

(63) Andrieux, C. P. ; Hapiot, P. ; Pinson, J. ; Savéant, J.M. Determination of formal potentials of chemically unstable redox couples by 2nd -harmonic alternating-current voltammetry and cyclic voltammetry – Application to the oxidation of thiophenoxide ions. *J. Am. Chem. Soc.* **1993**, *115*, 7783-7788.